Phenomenological Model of Current Sheet Canting in Pulsed Electromagnetic Accelerators

T.E. Markusic*
Propulsion Research Center
NASA Marshall Space Flight Center
Huntsville, AL 35812

E.Y. Choueiri†
Electric Propulsion and Plasma Dynamics Laboratory(EPPDyL)
Mechanical and Aerospace Engineering Department
Princeton University, Princeton, New Jersey 08544

IEPC 2003-0293‡

January 15, 2003

The phenomenon of current sheet canting in pulsed electromagnetic accelerators is the departure of the plasma sheet (that carries the current) from a plane that is perpendicular to the electrodes to one that is skewed (or tipped), which negatively impacts accelerator efficiency. In the present study, it is postulated that depletion of plasma near the anode, which results from axial density gradient induced diamagnetic drift, occurs during the early stages of the discharge, creating a density gradient normal to the anode, with a characteristic length on the order of the ion skin depth. Rapid penetration of the magnetic field through this region ensues, due to the Hall effect, leading to a canted current front ahead of the initial current conduction channel. Once the current sheet reaches appreciable speeds, entrainment of stationary propellant replenishes plasma in the anode region, inhibiting further Hall-convective transport of the magnetic field; however, the previously established tilted current sheet continues to drive plasma toward the cathode and accumulate it there. This proposed sequence of events has been incorporated into a phenomenological model. The model predicts that canting can be reduced by using low atomic mass propellants with high propellant loading number density; the model results are shown to give good agreement with experimentally measured canting angle mass dependence trends.

* Propulsion Research Scientist at the PRC. Member AIAA.
† Chief Scientist at EPPDyL. Associate Professor, Applied Physics Group. Senior Member AIAA.
‡ Presented at the 28^{th} International Electric Propulsion Conference, Toulouse, France, March 17-24, 2003.

Nomenclature

B - magnetic inductance [Gauss]
J - current density [A/cm^2]
$\mathbf{u}_\mathrm{d}$ - diamagnetic drift velocity [cm/s]
$\mathbf{v}_\mathrm{ba}$ - branch/anode interface velocity [cm/s]
$\mathbf{v}_\mathrm{bt}$ - branch/trunk interface velocity [cm/s]
c - speed of light in vacuum [cm/s]
e - electronic charge [statcoulomb]
I_sp - specific impulse [s]
L - trunk to anode separation [cm]
L_c - characteristic density gradient length [cm]
n_e - electron number density [#/cm^{-3}]
n_i - ion number density [#/cm^{-3}]
m_i - ion atomic mass [g]
R_c - convective skin effect Reynolds number
s - branch/trunk to branch/anode axial separation [cm]
v_A - Alfvén speed [cm/s]
v_c - Hall-convective speed [cm/s]
v_D - resistive diffusion speed [cm/s]
α - system mass per unit power [kg/kW]
δ_i - ion skin depth [cm]
η - plasma resistivity [Ωm]
θ - canting angle [degrees]
ω_p - plasma frequency [rad/s]

1 Introduction

Pulsed electromagnetic accelerators are devices which use intense bursts of electrical current [$\mathcal{O}(10^4 - 10^6)$ A] to create high speed [$\mathcal{O}(10^3 - 10^5)$ m/s] jets of plasma. They find application as plasma sources in many basic plasma science experiments[1] as well as in a specific genre of electric space propulsion device called the pulsed plasma thruster (PPT)[2]. The present work is motivated by the desire to improve the performance of pulsed electromagnetic accelerators in the context of plasma propulsion.

PPTs have the potential for fulfilling the attitude control requirements on a spacecraft at greatly reduced mass and cost. They are also being considered for constellation maintenance for missions such as interferometric imaging of the Earth from space or deep space from an Earth orbit (c.f., Polzin *et al*[3]). The benefits of PPTs are their simplicity, very small impulse bits for precise control of satellite motion, reliability, and high specific impulse. Two classifications of PPTs exist, corresponding to the form of propellant used: gas-fed (GFPPT) or ablative propellant (APPT). The gas-fed variety has the advantages of a "clean" exhaust plume and high specific impulse. The ablative version of the PPT uses a solid propellant, such as Teflon, to provide other advantages such as compactness and overall ease of system integration; however, plume contamination and lower specific impulse may limit the application of APPTs for some missions. The model presented in the present study is relevant to pulsed electromagnetic accelerators; it is therefore descriptive of all GFPPTs and, possibly, APPTs that operate in an electromagnetic acceleration regime[4].

2 Review of the Problem

2.1 Definition of the Problem

The phenomenon of current sheet canting is the departure of the current sheet from perpendicular attachment to the electrodes to a skewed, or tipped, attachment. It is best illustrated by an example. Figure 1 shows the evolution of a hypothetical and a real current sheet near the breech of a rectangular-geometry pulsed electromagnetic accelerator; outlines of the electrodes (the cathode is the bottom electrode) have been added for clarity. Ideally, we would like the current sheet to initiate at the breech, perpendicular to the electrodes, and remain so as it propagates axially (as illustrated on the left-hand side of the figure). In contrast, the right-hand side of the figure shows the experimentally observed evolution of a discharge[6]. As expected, the current sheet is seen to initiate at the breech; however, as time progresses, the current sheet is seen to severely tilt, or cant, as it propagates.

Canting creates off-axis components of thrust, which constitute a profile loss. Consider the t = 8 μs photograph on the right-hand side of Fig. 1. Assuming that the magnetic field is uniform behind the current sheet, the force on the top electrode (which is found by integrating the magnetic pressure on the electrode surface) will be greater than on the bottom electrode, because the top electrode has more surface area exposed to the magnetic field. This transverse force imbalance may result in an undesirable torque on a spacecraft which uses a PPT. Also, considering the work done by the current sheet, it is clear that a canted current sheet will apply a force to the propellant transverse to the thrust axis and thus expend energy which is not converted into useful thrust.

In addition to causing an off-axis component of thrust, current sheet canting may undermine the effective sweeping up of propellant as the current sheet propagates. The effect of canting may be to force the plasma entrained by the current sheet into the cathode where it stagnates and is then left behind. This behavior is suggested by interferometric data that shows a dense plasma layer along the cathode, that trails behind the current sheet[5]. Indeed, canted current sheets may act, undesirably, like *real* snowplows – never accumulating but, rather, throwing their

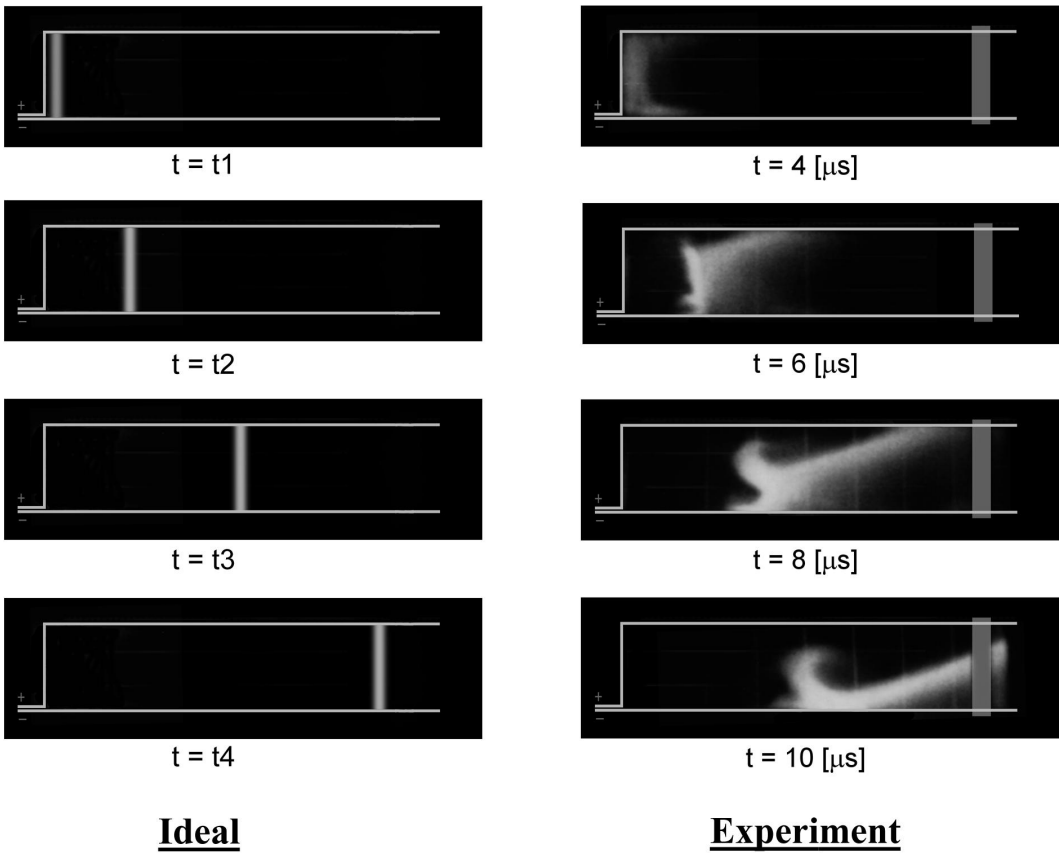

Figure 1: Comparison of ideal and experimentally observed current sheet propagation (from Markusic[5]). In the ideal case, it is implied that time t1<t2<t3<t4. The experimental photographs are from an argon (100 mTorr, uniform fill) discharge with peak current about 60 kA. Outlines of the electrodes have been added for clarity; the vertical rectangular element on the right-hand side of the pictures is a structural element that obstructed optical access.

load to the side as they pass by.

While direct studies of performance degradation due to current sheet canting are needed, the potentially adverse effects envisaged above provide reasonable justification for pursuing a theoretical study of the phenomenon. By developing an understanding of the physical processes which drive current sheet canting, we can develop prescriptions for how to reduce the effect, and ultimately provide guidance for the design of better pulsed plasma thrusters.

2.2 Review of Past Research

The literature from the early GFPPT researchers (see, for example, [7]-[11]) indicates that current sheet canting was a ubiquitous phenomenon – occurring in a variety of different electrode geometries and experimental conditions. However, detailed treatment of the subject is limited, with most references being anecdotal in nature. A review of the earlier studies can be found in Markusic[5]; the conclusions from that review can be summarized as follows:

- ➢ Current sheet canting always occurs in an orientation such that the anode current attachment leads the cathode current attachment.
- ➢ Current sheets are always observed to cant with nitrogen and argon propellant – irrespective of geometry (rectangular, coaxial, z-pinch, inverse z-pinch, and parallel rod), gas pressure, or current level.
- ➢ Uncanted hydrogen and deuterium current sheets have been observed but only with specially prepared electrodes.
- ➢ Ion current conduction is believed to play an important role in establishing the overall current pattern.

➢ Current sheets appear to exhibit invariant features (e. g. anode foot, cathode hook, and canting) over a wide range of geometries, propellent species, gas pressures, and current levels.

3 Model Description

Below we present a phenomenological model for canting that is motivated by the observations listed above as well as recent experimental measurements of current sheet canting angles for a variety of propellants[5].

3.1 Current Conduction Phases

After initiation, the evolution of a current sheet in an electromagnetic accelerator can be divided into three phases: starvation, branching, and snowplow phases. Figure 2 schematically illustrates this evolution. Corresponding photographs from the experimental study[5] are shown at the top of the figure. The grey objects in the illustrations are meant to illustrate the spatial extents of the current sheet plasma. The solid lines behind the current sheet are meant to represent magnetic flux tubes (i.e., the amount of magnetic flux contained between consecutive pairs of lines is constant from frame-to-frame).

The first illustration in Fig. 2 shows the initiation of the current sheet at the breech of the accelerator. In illustration 2 the current sheet is shown shortly after initiation. The plasma in the region near the anode becomes severely depleted due to mass motion of the fluid toward the cathode (for reasons to be explained later). This first phase is termed the "starvation phase", borrowing terminology from a phenomenon observed in MPD thrusters called "anode starvation" (which is due to a somewhat different physical mechanism)[12].

Between illustrations 2 and 3 the plasma near the anode becomes so tenuous that it can no longer contain the magnetic field behind it. In a sense the current sheet can be thought of as a thin membrane (like a balloon) that contains a high pressure "magnetic fluid". When the plasma near the the anode becomes sufficiently "thin", the membrane quickly expands, or ruptures, allowing the contained magnetic flux to rapidly stream through. The initial current channel (henceforth referred to as the "trunk") becomes bifurcated along the anode, as the streaming magnetic flux (and associated surface current) propagate ahead of the original current attachment point; this interface forms a new conduction path for the current sheet which connects the trunk to the anode (this new conduction path will be referred to as the "branch"). The newly formed branch and trunk form what was referred to by earlier researchers as the "anode foot". Eventually the trunk becomes magnetically insulated (as the magnetic field wraps around the top of the trunk, transport from the top of the trunk to the anode is impeded by the transverse magnetic field) from the anode whereupon all of the current flows through the branch.

The branch propagates, borrowing from shock-tube parlance, as a contact discontinuity, with the anode as one wall and the trunk as the other. The magnetic pressure drives the contact point down along the branch-trunk interface and forward along the branch-anode interface, resulting in a canted current sheet. Anode starvation occurs to a lesser extent in the branch because it continually propagates into a fresh supply of propellant (the branch-anode interface is replenished with propellant from the *dynamic* pressure associated with its substantial axial speed). On the other hand, the initial current sheet (the trunk), is unable to avoid anode starvation because of its slow initial speed. As a final note on the branching phase, the magnetic pressure between the branch and the trunk causes the trunk to deform into the hook-like structure reported in many studies; the hook is simply a vestige of the initial current sheet.

The branching phase ends when the bottom of the branch reaches the cathode and the final phase (as shown in illustration 5), the snowplow phase, begins. The magnetic pressure is uniformly distributed on the back face of the canted current sheet and the current sheet is sufficiently dense in all areas to prevent further field leakage. The current sheet thus remains at a fairly constant canting angle during the remainder of its propagation. The tilt of the current sheet causes it to exert a cathode-directed component of the $\mathbf{J} \times \mathbf{B}$ force density on all of the propellant which is subsequently swept up. As a result, the propellant is preferentially directed toward the cathode, where it accumulates. This "mass-funnelling" may cause elevated plasma pressure along the cathode – leading to expansion of the propellant into the region *behind* the current sheet. A structure in the form of a plasma "bubble" behind the current sheet could form and, over time, grow large enough to span the entire gap between the anode and cathode and cause a "restrike", which effectively short circuits the initial current sheet.

3.2 Terminal Canting Angle

Current sheet canting results from a disparity in the axial propagation speed between the branch-anode and branch-trunk interfaces. The branch-anode interface moves faster and the current channel connecting the anode to the trunk forms a canted current sheet.

The canting angle, $\theta(\tau)$, continuously evolves from zero to its terminal (final) value, θ_f, during the branch-

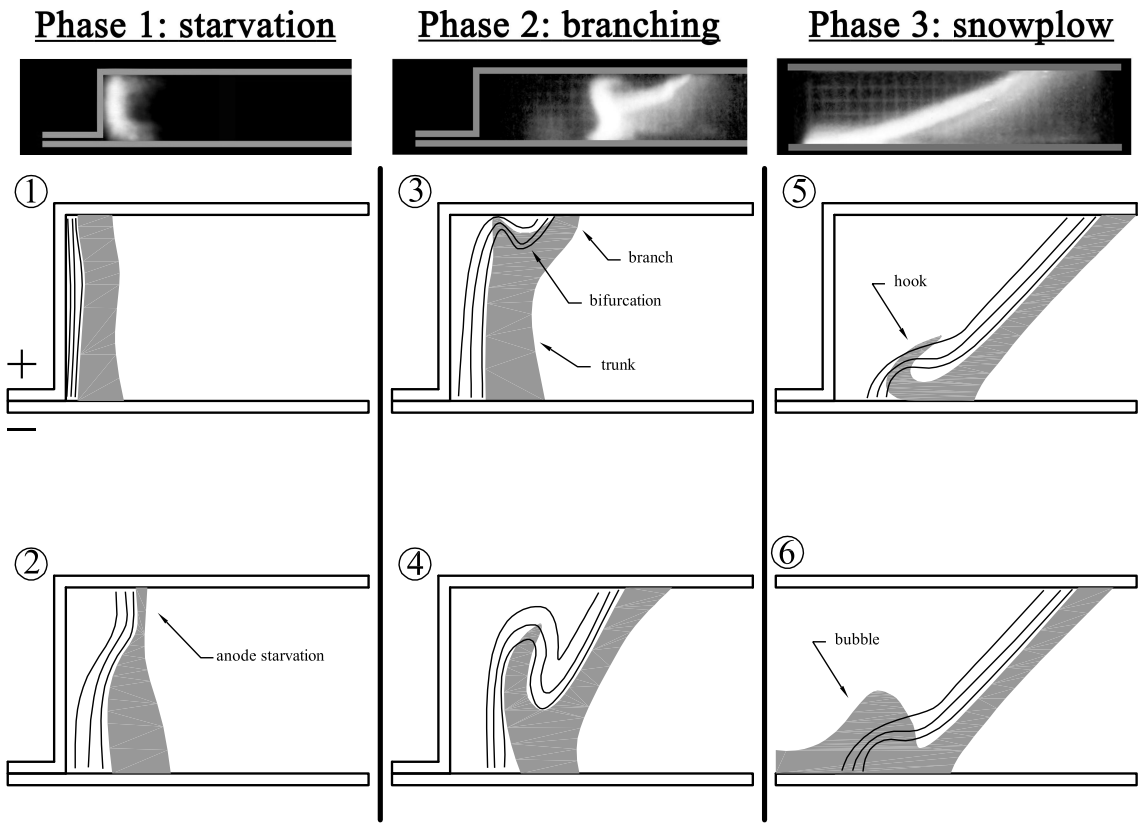

Figure 2: Illustration of a model showing current conduction phases which lead to a canted current sheet.

ing phase. The severity of the canting depends on the relative magnitude of the branch-anode and branch-trunk interface velocities. The terminal canting angle can be predicted by calculating the trajectories of two points on the branch: the branch-trunk interface point (point BT) and the branch-anode interface point (point BA). The elements of the model are schematically illustrated in Fig. 3. The figure shows "snapshots" of the current sheet at several different times. The branch comes into existence at some time $t_\circ$; the points BA and BT are assumed to initially be separated by the distance L. The point BA moves with velocity $\mathbf{v}_{\rm ba} = |\mathbf{v}_{\rm ba}|\hat{x}$. The point BT has two velocity components, $\mathbf{v}_{\rm bt} = |\mathbf{v}_{\rm bt}|\sin\theta\hat{x} + |\mathbf{v}_{\rm bt}|\cos\theta\hat{y}$, because the flux tubes that wrap around this point (see frames 3 and 4 of Fig. 2) exert both axial and transverse components of magnetic pressure, driving the point both forward and downward. The branching phase is assumed to terminate when the point BT reaches the cathode (indicated by time t_f in the figure). The predicted terminal canting angle (θ_f) is calculated using the axial separation of the points BA and BT (s in the figure) at time t_f. For a given electrode separation distance h:

$$\theta_f = \tan^{-1}\left(\frac{\rm s}{\rm h}\right) \ , \tag{1}$$

$$\rm s = \int_0^{t_f} (|\mathbf{v}_{ba}| - |\mathbf{v}_{bt}|\sin\theta)d\tau \ , \tag{2}$$

$$\rm h - L = \int_0^{t_f} |\mathbf{v}_{bt}|\cos\theta d\tau \ . \tag{3}$$

Assuming $|\mathbf{v}_{\rm ba}|$ and $|\mathbf{v}_{\rm bt}|$ are known, Eqns. 1-3 can be numerically integrated to yield the predicted canting angle. The values of $|\mathbf{v}_{\rm ba}|$ and $|\mathbf{v}_{\rm bt}|$ must come from physical models that describe current sheet propagation. In the next section we make arguments for the appropriate choice of values for these constants.

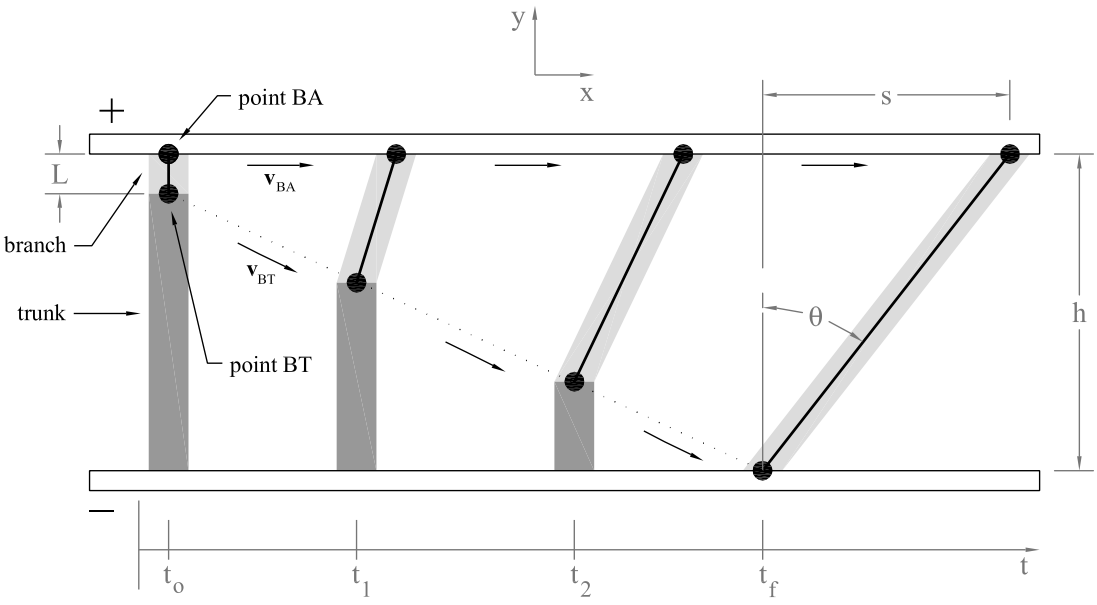

Figure 3: Schematic of current sheet canting angle calculation elements (rectangular geometry).

4 Current Sheet Propagation

4.1 Propagation Speed

An ideal current sheet forms at the discontinuity between a vacuum region filled with expanding magnetic flux and a conductive, relatively flux-free plasma. The extent to which the magnetic field penetrates into the plasma depends on the thermodynamic state of the plasma. Classically, two extreme cases can be distinguished. If the plasma is highly conductive, the penetration of the fields is confined to a thin layer of thickness on the order of the electron skin depth and the plasma is pushed by the magnetic pressure (snowplowed) with a characteristic speed given by the Alfvén speed[13],

$$v_{\mathrm{A}} \equiv \frac{B}{\sqrt{4\pi n_i m_i}} \,, \tag{4}$$

where B is the magnetic inductance, n_i is the ion density, and m_i is the atomic mass of the ions. If, on the other hand, the plasma is highly resistive, the magnetic field simply diffuses through the plasma (without imparting significant momentum) with characteristic speed[13]

$$v_{\mathrm{D}} \equiv \frac{c^2 \eta}{4\pi L_{\mathrm{D}}} \,, \tag{5}$$

where c is the speed of light in vacuum, η is the plasma resistivity, and L_{D} is the characteristic diffusion length.

4.2 Hall Effect Enhanced Field Penetration

Fruchtman *et al.*[14, 15, 16] describe a mechanism for fast magnetic field penetration into a plasma which is *independent* of the resistivity, and which they call the "convective skin effect". The mechanism results from the Hall electric field, which allows the magnetic field to penetrate the plasma with characteristic speed

$$v_c \equiv \frac{c^2 (B/n_e e c)}{4\pi L_{\mathrm{c}}} \,, \tag{6}$$

where $-e$ is the electron charge and L_{C} is the characteristic length of a density gradient (transverse to the propagation direction) in the plasma. The term $\eta_H = B/n_e e c$ can be thought of as a "Hall resistivity". As with conventional plasma resistivity, the Hall resistivity allows the magnetic field to rapidly propagate through a plasma without imparting significant momentum to the ions (the Hall resistivity is, however, non-dissipative). The Hall effect-enhanced magnetic field penetration will occur when a density gradient occurs in the (pushed) plasma with char-

acteristic dimension of the order of the ion skin depth,

$$\delta_i \equiv \sqrt{\frac{m_i c^2}{4\pi n_i e^2}} \,. \tag{7}$$

Also, a parameter equivalent to the magnetic Reynolds number can be defined, which is the ratio of the plasma pushing speed ($v_{\rm A}$) to the field penetration speed (v_c):

$$R_c \equiv \frac{v_{\rm A}}{v_c} = \sqrt{\frac{4\pi n_i e^2}{m_i c^2}}\, L_{\rm c} = \frac{L_{\rm c}}{\delta_i} \,. \tag{8}$$

Equation 8 shows us that when $L_{\rm C}$ is less than the ion skin depth, field penetration dominates over pushing.

4.3 Diamagnetic Drift and Anode Starvation

The sequence of events, described in section 3.1, that lead to a canted current sheet are initiated by depletion of the conducting plasma in the vicinity of the anode. In this section we describe one mechanism that may drive this depletion process: diamagnetic drift.

One of the most conspicuous physical traits of current sheets are the large gradients in both the field strengths and thermodynamic state variables that occur across it. It is therefore natural to first check the influence of these abrupt transitions on the phenomenon of interest. In current sheets the gasdynamic pressure and magnetic field gradients are generally quite large. Plasma pressure gradients transverse to magnetic fields gives rise to motion of the plasma in a direction perpendicular to both the **B** field and the pressure gradient. For example, a simplified version of the fluid momentum equation for the j_{th} plasma species gives the component of velocity perpendicular to the magnetic field[17]:

$$\mathbf{u}_{\perp j} = \underbrace{\frac{\mathbf{E}\times\mathbf{B}}{B^2}}_{\mathbf{u}_E} - \underbrace{\frac{\nabla p_j \times \mathbf{B}}{q_j n_j B^2}}_{\mathbf{u}_d} \,. \tag{9}$$

The first term in Eqn. 9 is the $\mathbf{E}\times\mathbf{B}$ drift ($\mathbf{u}_E$) and the second term is the diamagnetic drift ($\mathbf{u}_d$). The direction of $\mathbf{u}_E$ is the same for both ions and electrons but the diamagnetic drift direction is seen to be charge dependent. With the anode on top as illustrated in Fig. 3, $\mathbf{E}$ is directed in the $-\hat{y}$ direction, and $\mathbf{B}$ is directed in $-\hat{z}$ direction so that $\mathbf{u}_E$ is directed in the $+\hat{x}$ direction. Similarly, with ∇p in the $+\hat{x}$ direction, for ions, $\mathbf{u}_d$ is directed in the $-\hat{y}$ direction, or away from the anode throughout the current sheet.

Since most of the plasma inertia is carried by the ions, the simplified analysis above indicates that current sheets with large pressure gradients in the axial direction will induce fluid flow away from the anode. We propose that this mass motion can lead to anode starvation and the Hall-enhanced **B** field penetration described in the previous section. The speed of the current sheet along the anode will be given by Eqn. 6. In order to calculate the Hall-convective speed, the scale length, $L_{\rm c}$, for the diamagnetic drift induced density gradient normal to the anode must be known. In the analytical theory of Fruchtman[14], this scale length is defined as $L_{\rm c} = \{({\rm d}/{\rm d}y)\ln[n_e(y)]\}^{-1}$. In order to make canting angle predictions either the functional form of the electron distribution near the anode must be provided from a model, or scale length estimates can be made using experimental data.

5 Model Results

Referring again to Fig. 3, if we assume that the branch-trunk interface motion is governed by plasma pushing ($|\mathbf{v}_{\rm bt}| = v_{\rm A}$), and that the branch-anode interface motion is governed by Hall-convective transport ($|\mathbf{v}_{\rm ba}| = {\rm v}_c$), then Eqns. 1-3 can be integrated to yield the canting angle for a given propellant atomic mass, ion number density and characteristic density gradient length.

If we simplify the model by assuming h$\gg$L and eliminate the instantaneous angular (θ) dependence of the point BT trajectory by assuming that $\mathbf{v}_{\rm bt} = v_{\rm A}\hat{x} + v_{\rm A}\hat{y}$, the predicted canting angle can be written in closed form:

$$\theta_f = \tan^{-1}\left(\frac{1-R_{\rm c}}{R_{\rm c}}\right) \,. \tag{10}$$

This approximate expression is found to yield canting angle values to within $\sim\pm$25% of the numerically integrated results.

The numerically integrated model results are displayed in Fig. 4. Contours of constant canting angle for the the atomic mass and number density regime of interest for GFPPTs are plotted. We have fixed h=5 cm and L_c=0.1 cm, which are typical values for a GFPPT, as discussed below. The model predicts increased canting with increasing atomic mass and decreasing number density.

5.1 Comparison with Experiment

In an earlier study[5] we measured (using interferometry and magnetic field probes) the canting angle of current sheets using a variety of different propellants (hydrogen, deuterium, methane, helium, neon, argon, krypton, and xenon) and pressure levels (75, 200, and 400 mTorr). The accelerator was rectangular in geometry, with dimensions 5×10×60 cm (height×width×length). We also measured the current sheet speed, B-field, electron density, and electron temperature. These data can be used to estimate $v_{\rm A}$ and v_c. The diamagnetic drift speed was estimated to be

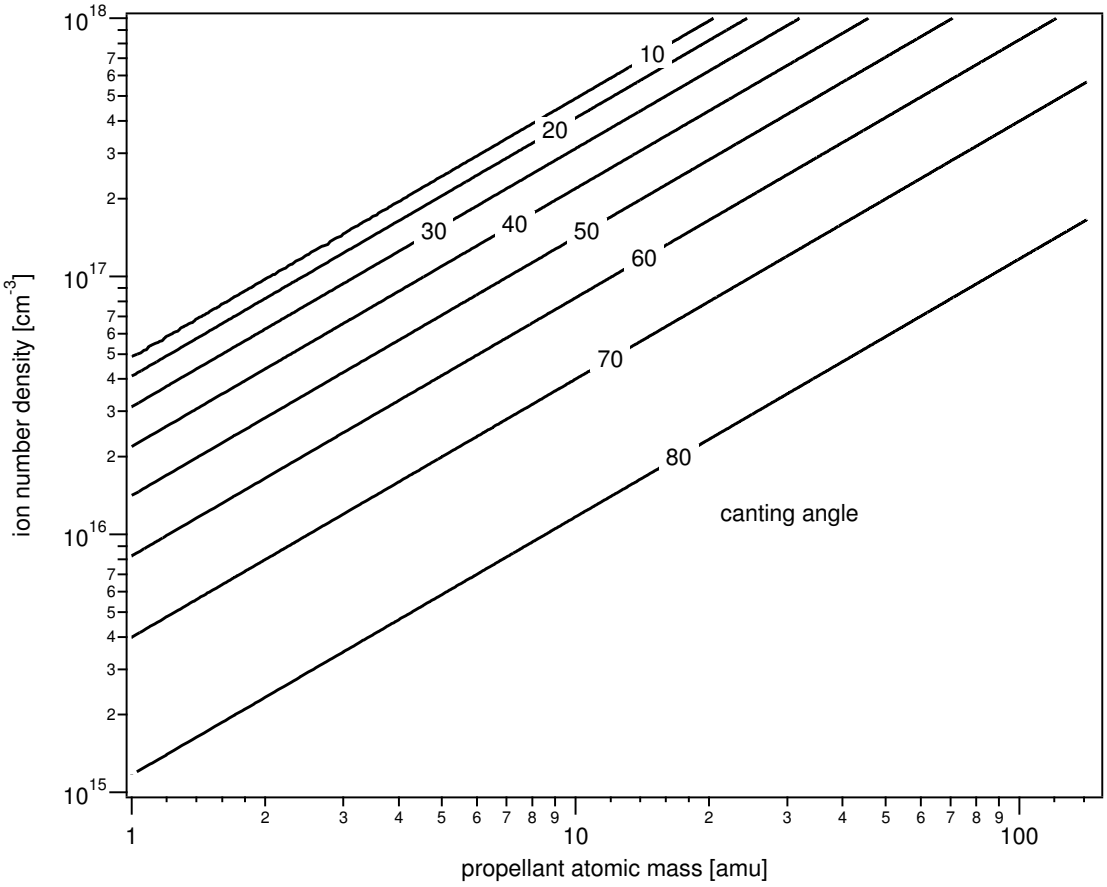

Figure 4: Canting model results: contours of constant canting angle (h=5 cm, $L_c = 0.1$ cm).

$|\mathbf{u}_d| \sim \mathcal{O}(10^{-3})$ m/s. The characteristic time for the branching phase was observed to be $t_b \sim \mathcal{O}(10^{-6})$ s, which implies that diamagnetic drift is capable of displacing plasma away from the anode about $|\mathbf{u}_d| t_b \sim 0.1$ cm during the branching phase. Therefore, we take $L_c \sim 0.1$ cm as the order of magnitude of the near-anode density gradient. The magnitude of this characteristic length is perhaps not surprising, since the experimental measurements yield a comparable estimate for the *axial* characteristic length, $n/\nabla n$. Using the electron density data we found that $n/\nabla n \sim 0.1$ cm for all cases, which is the same order of magnitude as our estimated *normal* characteristic length.

Using the average experimentally measured number density ($\sim 1 \times 10^{16}$ cm^{-3}) and the diamagnetic drift-induced characteristic density gradient length ($L_c \sim 0.2$ cm), we can calculate the predicted canting angle as a function of the propellant atomic mass. This curve, along with all of the experimental data points are shown in figure 5. The figure shows that the model captures the general trend of the experimental data; the model predicts that the canting angle will initially rapidly increase with propellant atomic mass and then taper off toward a more asymptotic trend for higher atomic mass propellants. These are the same trends that are seen in the experimental data.

It is not surprising that the model does not give precise quantitative agreement with the data for the higher atomic mass propellants. The model predicts the "worst case scenario", or *maximum* expected canting angle, because the simplification in the model that allows the point BA to propagate with velocity v_c along its entire trajectory probably does not completely capture the complexity of the actual near-anode behavior. In the real accelerator, the branch anode attachment is likely to transition continuously from the Hall-convective behavior back to plasma pushing – as it picks up speed and the incoming propellant obliterates the anode density gradient. If we were to modify the model to divide the branch trajectory

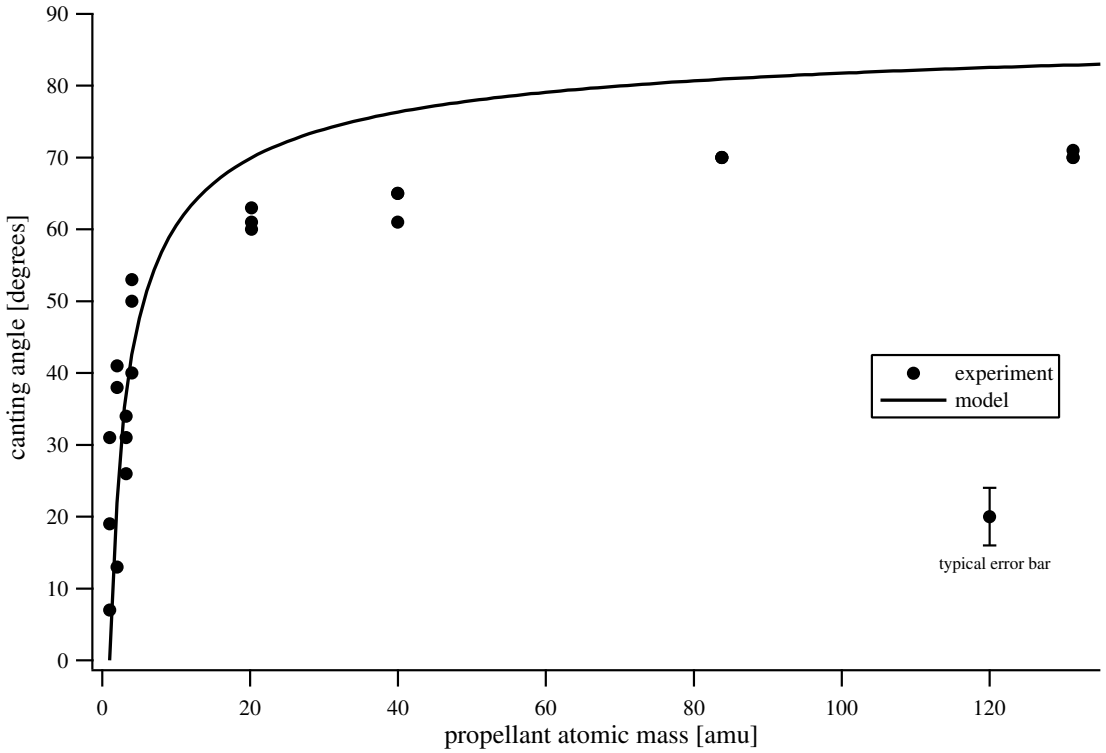

Figure 5: Comparison of model and measured current sheet canting angle[5] versus propellant atomic mass.

into, say, two parts (half Hall-convective and half plasma pushing), the effect would be to cause the model curve to bend-over more rapidly and come into closer agreement with the data. But, in light of the rather crude order of magnitude estimates used throughout this analysis, further refinement of the model is not warranted. The important point is that the simplest model, which embodies the essence of the proposed physical processes, accurately picks up the trends in the experimental data and gives fairly close quantitative agreement.

6 Discussion and Conclusions

The proposed current sheet canting model can be summarized as follows. Physically, Fruchtman's model[15] shows that the Hall effect can lead to an effective mechanism for magnetic field transport when a non-uniformity (i.e., a density gradient) appears in a plasma that is being pushed by the field. This argument is formally derived through the EMHD fluid equations[14]. In particular, inclusion of the Hall term in the generalized Ohm's law leads to a term in the equation for the time-evolution of the magnetic field that allows for the rapid convection of magnetic field through the plasma, without displacement of the ions, with characteristic speed v_{c}. This competes with the convection of the magnetic field where the ions are displaced, that is plasma pushing, which has characteristic speed v_{A}. Consideration of the relative magnitude of each effect reveals that the Hall-convective penetration becomes comparable in magnitude to plasma pushing when a density gradient of scale length comparable to the ion skin depth appears.

In our fast field penetration canting model we propose that such a density gradient does arise along the anode of the accelerator due to diamagnetic drift, allowing localized rapid penetration of the magnetic field and the formation of two distinct current carrying structures, which we call the branch and the trunk. Current sheet canting results from a disparity in the axial propagation speed between the branch-anode and branch-trunk interfaces. The branch-anode interface moves faster and the current channel connecting the anode to the trunk forms a canted current sheet. The canting angle continuously evolves from zero to its terminal value during the branching phase. The severity of the canting depends on the relative magnitude the branch-anode and branch-trunk interface velocities. The variations in the ion skin depths among the different

propellants (the ion skin depth is proportional to $\sqrt{\mathrm{m_i}/\mathrm{n_i}}$) leads to different Hall-convective field penetration speeds, and hence different final canting angles.

The results of this study provide practical guidance. In coaxial accelerators a simple design rule can immediately be stated: the outer electrode should always be the anode. In the coaxial geometry, the $1/r^2$ variation in magnetic pressure predisposes the current sheet to run faster along the inner electrode; by making the inner electrode the anode, this undesirable situation would only be amplified because of the natural tendency of the current sheet to move faster along the anode. But, if the outer electrode is made to be the anode, some antagonism between the two effects might be established wherein the non-uniform magnetic pressure effect could be counteracted by the tendency of the current sheet to move faster along the anode, leading to a non-canted current sheet.

GFPPTs should use low atomic mass propellants at high pressure to avoid performance losses due to current sheet canting. Hydrogen would seem to be the best choice; however, hydrogen is not an ideal PPT propellant, due to the difficulty of handling cryogenic propellants on a spacecraft. To practically exploit the benefits of low current sheet canting which results from the use of hydrogen at high pressure, alkanes, with their hydrogen-rich $C_N H_{2N+2}$ structure, may be a natural choice. Methane was tested as part of the experimental study and was found to have the same reduced canting behavior (at higher pressures) as hydrogen. Further tests are needed on longer-chain hydrocarbons. If butane, for example, is found to exhibit similar behavior, it will be an appealing GFPPT propellant on two levels. In addition to the aforementioned canting benefits, butane can be stored as a liquid under relatively low pressure, at room temperature; therefore, a butane propellant system will have a much smaller specific volume (smaller fuel tank and feed system) than a high pressure gas system, and provide a lower overall system α.

References

[1] J. Marshal. Performance of a hydromagnetic plasma gun. *The Physics of Fluids*, 3(1):134–135, January-February 1960.

[2] R.G. Jahn. *Physics of Electric Propulsion*. McGraw-Hill Book Company, 1968.

[3] K.A. Polzin, E.Y. Choueiri, P. Gurfil, and N.J. Kasdin. Plasma propulsion options for multiple terrestrial planet finder architectures. *Journal of Spacecraft and Rockets*, 39(3):347–356, 2002.

[4] D.R. Keefer and B. Rhodes. Electromagnetic acceleration in pulsed plasma thrusters. In 25^{th} *International Electric Propulsion Conference*, Cleveland, OH, August 1997. IEPC 97-035.

[5] T.E. Markusic. *Current Sheet Canting in Pulsed Electromagnetic Accelerators*. PhD thesis, Princeton University, 2002.

[6] T.E. Markusic and E.Y. Choueiri. Visualization of current sheet canting in a pulsed plasma accelerator. In 26^{th} *International Electric Propulsion Conference*, Kitakyushu, Japan, October 17-21 1999. IEPC 99-206.

[7] J.C. Keck. Current distribution in a magnetic annular shock tube. *The Physics of Fluids*, 5:630–632, 1962.

[8] F.J. Fishman and H. Petschek. Flow model for large radius-ratio magnetic annular shock-tube operation. *The Physics of Fluids*, 5:632–633, 1962.

[9] R.B. Johansson. Current sheet tilt in a radial magnetic shock tube. *The Physics of Fluids*, 8(5):866–871, 1964.

[10] R.H. Lovberg. The measurement of plasma density in a rail accelerator by means of schlieren photography. *IEEE Transactions on Nuclear Science*, pages 187–198, January 1964.

[11] R.L. Burton. *Structure of the Current Sheet in a Pinch Discharge*. PhD thesis, Princeton University, 1966.

[12] K.D. Diamant. *The anode fall in a high power pulsed MPD thruster*. PhD thesis, Princeton University, 1996.

[13] N.A. Krall and A.W. Trivelpiece. *Principles of Plasma Physics*. San Franscisco Press, 1986.

[14] A. Fruchtman. Penetration and expulsion of magnetic fields in plasmas due to the hall field. *Phys. Fluids B*, 3(8), 1991.

[15] A. Fruchtman. The snowplow in plasmas of nonuiform density. *Phys. Fluids B*, 4(4), 1992.

[16] A. Fruchtman and K. Gomberoff. Magnetic field penetration due to the hall field in (almost) collisionless plasmas. *Phys. Fluids B*, 5(7), 1993.

[17] L. Spitzer. *Physics of fully ionized gases*. Interscience Publishers, 1962.